Title: Corrosion properties of Ca65-xMg17.5Zn17.5+x (x = 0, 2.5, 5) alloys

Author: R. Babilas, P. Wojciechowski, Anna Bajorek, P. Sakiewicz, K. Cesarz-Andraczke

Citation style: Babilas R., Wojciechowski P., Bajorek Anna, Sakiewicz P., Cesarz-Andraczke K. (2019). Corrosion properties of Ca65-xMg17.5Zn17.5+x (x = 0, 2.5, 5) alloys. "Archives of Metallurgy and Materials" (2019, no. 3, s. 1033-1040), doi 10.24425/amm.2019.129492

www.czasopisma.pan.pl PAN POLSKA AKADEMIA NAUK www.journals.pan.pl

Arch. Metall. Mater. **64** (2019), 3, 1033-1040

DOI: 10.24425/amm.2019.129492

R. BABILAS*#, P. WOJCIECHOWSKI*, A. BAJOREK**, P. SAKIEWICZ*, K. CESARZ-ANDRACZKE*

CORROSION PROPERTIES OF $Ca_{65-x}Mg_{17.5}Zn_{17.5+x}$ (x = 0, 2.5, 5) ALLOYS

The aim of the paper is to study the effect of zinc addition on the corrosion behavior of $Ca_{65-x}Mg_{17.5}Zn_{17.5+x}$ (x = 0, 2.5, 5 at.%) alloys in simulated physiological fluids at 37°C. The electrochemical measurements allowed to determine a corrosion potential, which showed a positive shift from –1.60 V for $Ca_{65}Mg_{17.5}Zn_{17.5}$ alloy to –1.58 V for $Ca_{60}Mg_{17.5}Zn_{22.5}$ alloy, adequately. The more significant decrease of hydrogen evolution was noticed for $Ca_{60}Mg_{17.5}Zn_{22.5}$ alloy (22.4 ml/cm^2) than for $Ca_{62.5}Mg_{17.5}Zn_{20}$ and $Ca_{65}Mg_{17.5}Zn_{17.5}$ samples (29.9 ml/cm^2 and 46.4 ml/cm^2), consequently. The corrosion products after immersion tests in Ringer's solution during 1 h were identified by X-ray diffraction and X-ray photoelectron spectroscopy as calcium, magnesium oxides, carbonates, hydroxides and calcium hydrate.

Keywords: Ca-based alloys; Corrosion; Hydrogen evaluation; X-ray photoelectron spectroscopy

1. Introduction

In classification of amorphous materials proposed by Takeuchi and Inoue [1], the Ca-based alloys represent a new group of bulk metallic glasses (BMGs). The BMGs consist of simple alkaline metals (Ca and Mg) and late transition metals (Ag, Cu, Zn, Ni). The Ca-based amorphous alloys due to their promising properties and biocompatibility can be also examined as a new class of biomaterials. The biocompatible elements such as Ca, Mg and Zn caused that these alloys can be used as resorbable implants. The zinc addition in Ca-Mg-Zn alloys is considered as a grain refiner, therefore it enhanced a strength of alloy [2]. The magnesium alloys with Zn addition revealed improved corrosion properties compared to pure Mg. The minor addition of Ca (0.5-0.7 wt.%) caused the increase of corrosion and mechanical properties in binary magnesium alloys [3]. Biocompatible corrosion products can be resorbed by human body. Therefore, new Ca-based [4,5], Mg-based [6-9], Zn-based [10,11], Sr-based [12], Fe-based [13,14] and Zr-based [15,16] metallic glasses with biocompatible chemical composition were examined as resorbable materials. Thanks to a biocompatibility, Ca-based metallic glasses are developed for biomedical application. For example, in vitro and in vivo studies showed that high entropy metallic glasses as $Ca_{20}Mg_{20}Zn_{20}Sr_{20}Yb_{20}$ could stimulate and promote osteogenesis and a new bone formation [17].

The elastic modulus, tensile and compressive strength or ductility of biomaterials determinate design and fabrication method of the prosthesis. The Ca-based metallic glasses show favorable properties in relation to medical applications due to their low density (2-4 g/cm^3) and low Young's modulus (20-46 GPa) [18-20]. In addition, a critical diameter of Ca-Mg-Zn metallic glasses achieved a value of 15 mm. The metallic glasses can be prepared by using a conventional copper mold casting [21,22]. The lack of defects like grain boundaries and compositional homogeneity of amorphous structure increases resistivity for oxidation. It should be noted, that factors like stress and temperature can reveal influence on stability of amorphous structure and caused crystallization [23]. The most important drawback of Ca-Mg-Zn metallic glasses is relatively rapid degradation rate, which resulted in a loss of mechanical properties. The calcium and magnesium are very active and react with water generating hydrogen gas and hydroxides. The high corrosion rate is another barrier to use Ca-based metallic glasses as resorbable implants, because the human body is a rather aggressive environment. The human blood is dynamic, oxygenated saline solution with NaCl content of 0.9 wt.%, pH of 7.4 and temperature about 37°C [24]. The content of chlorides and pH of corrosive fluid is also important. Therefore, in the present work corrosion studies of Ca-based alloys in selected biocorrosive fluids were conducted.

2. Experimental

The studies were performed on $Ca_{65-x}Mg_{17.5}Zn_{17.5+x}$ (x = 0, 2.5, 5 at.%) alloys in the form of plates. The plates with a length and a width of 10 mm as well as a thickness of 1 mm were prepared by the pressure die casting [19]. The master alloys were

* SILESIAN UNIVERSITY OF TECHNOLOGY, INSTITUTE OF ENGINEERING MATERIALS AND BIOMATERIALS 18A KONARSKIEGO STR., 44-100 GLIWICE, POLAND
** UNIVERSITY OF SILESIA, A. CHELKOWSKI INSTITUTE OF PHYSICS, 4 UNIWERSYTECKA STR., 40-007 KATOWICE, POLAND
# Corresponding author: rafal.babilas@polsl.pl

produced by induction melting. The identification of structure and phase analysis of corrosion products after corrosion tests was provided by the X-ray diffraction (XRD) using the diffractometer with Co *K*α radiation. The diffraction patterns were collected by "step-scanning" method in a range from 30° to 90° of *2θ* angle.

The corrosion activity of the alloys was determined by results of hydrogen evolution volume and electrochemical measurements. The immersion tests and electrochemical measurements were conducted in physiological fluid (5.75 g/dm^3 NaCl, 0.38 g/dm^3 KCl, 0.394 g/dm^3 $CaCl_2$, 0.2 g/dm^3 $MgCl_2$, 0.9 g/dm^3 $C_6H_5Na_3O_7 \cdot 2H_2O$) and Ringer's solution (8.6 g/dm^3 NaCl, 0.3 g/dm^3 KCl, 0.48 g/dm^3 $CaCl_2$) at 37°C. The potentiodynamic measurements were conducted using the three-electrode cell. The cell was equipped with a working electrode (sample), a reference electrode (saturated calomel electrode, SCE) and a counter electrode (platinum rod). The corrosion resistance of the studied samples was evaluated by recording of the open-circuit potential (E_{OCP}) changes in a function of time and polarisation curves in the potential range E_{OCP} – 250 mV to E_{OCP} + 250 mV. The corrosion potential (E_{corr}), corrosion current density (j_{corr}) and polarisation resistance (R_p) was also determined according to Stern-Geary approach.

Electronic structure of $Ca_{60}Mg_{17.5}Zn_{22.5}$ sample after immersion test Ringer's solution was determined by use of X-ray photoelectron spectroscopy (XPS) technique. The Physical Electronics (PHI 5700/660) spectrometer working in ultra-high vacuum (10^{-9} Torr) conditions and monochromatic Al *K*α X-ray source (1486.6 eV) was used. The samples for XPS experiments were kept under vacuum for 12 h. Afterwards, the survey spectra were measured with the pass energy 187.85 eV. As a next step the depth profiles (DP-XPS) analysis were carried out by using 1.5 kV Ar+ beam for 15 minutes sputtering at intervals between measurements. At the end of etching process (after 315 minute of total sputtering time) the survey spectra were also recorded for comparison with the surface one. All the core level lines were measured with the pass energy 23.5 eV and with a standard limit of 0.1 eV resolution. All spectra were determined relative to the C1s peak (EB = 284.8 eV) as an adventitious carbon usually accumulated on the surface of the sample and used as a reference for charge correction.

The changes of surface morphology of the samples in as-cast state and after immersion tests in Ringer's solution were analyzed using a light microscope.

3. Results

X-ray diffraction results confirmed that examined $Ca_{65-x}Mg_{17.5}Zn_{17.5+x}$ (x = 0, 2.5, 5 at.%) samples in as-cast state show mostly amorphous structure with crystalline peaks. The broaden diffraction peak in 2-theta range from 38 to 43° was noticed (Fig. 1). However, the XRD patterns of $Ca_{65-x}Mg_{17.5}Zn_{17.5+x}$ (x = 0, 2.5, 5 at.%) plates in as-cast state show also single diffraction lines probably come from CaZn2 and Ca3Zn crystalline phases.

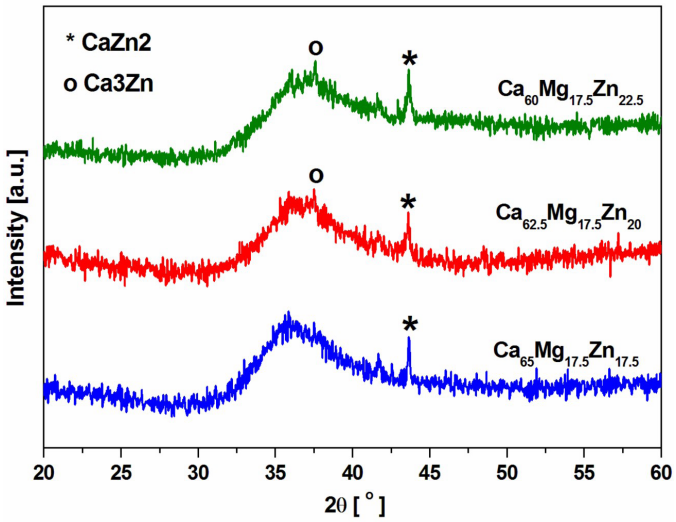

Fig. 1. XRD patterns of $Ca_{65-x}Mg_{17.5}Zn_{17.5+x}$ (x = 0, 2.5, 5 at.%) plates in as-cast state

The immersion tests of $Ca_{60}Mg_{17.5}Zn_{22.5}$, $Ca_{62.5}Mg_{17.5}Zn_{20}$ and $Ca_{65}Mg_{17.5}Zn_{17.5}$ alloys in Ringer's solution at 37°C present hydrogen evolution volume collected during 7 h (Fig. 2). In beginning stage of the immersion (up to 2 h) the H_2 evolution volume is relatively high for all studied alloys. The significantly less volume of the H_2 after 7 h was noticed for $Ca_{60}Mg_{17.5}Zn_{22.5}$ alloy (22.4 ml/cm^2) than for $Ca_{62.5}Mg_{17.5}Zn_{20}$ and $Ca_{65}Mg_{17.5}Zn_{17.5}$ samples (29.9 ml/cm^2 and 46.4 ml/cm^2), adequately.

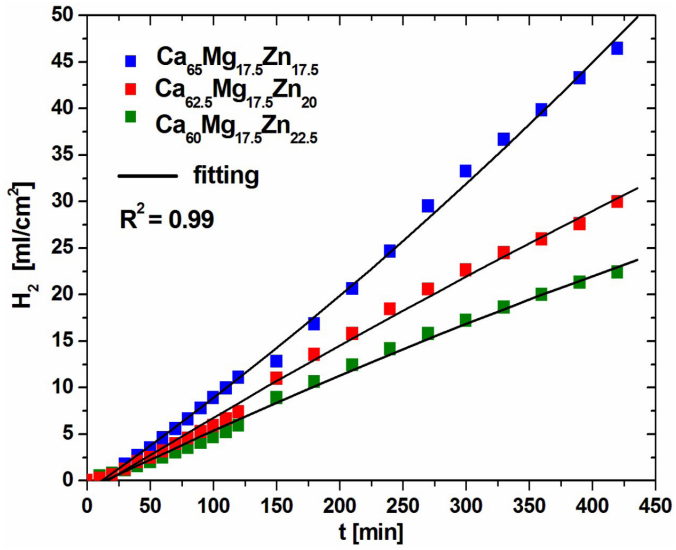

Fig. 2. Hydrogen evolution volume of $Ca_{65-x}Mg_{17.5}Zn_{17.5+x}$ (x = 0, 2.5, 5 at.%) alloys in Ringer's solution at 37°C

The changes of open circuit potential (E_{OCP}) after 3600 s of immersion in physiological fluid and Ringer's solution at 37°C are shown in Fig. 3. The more positive value of the E_{OCP} was detected for samples immersed in the physiological fluid rather than in Ringer's solution (Table 1,2). The major changes the E_{OCP} were noticed for $Ca_{62.5}Mg_{17.5}Zn_{20}$ alloy (Fig. 3b). Similarly, slightly changes of the E_{OCP} was noticed for

$Ca_{65}Mg_{17.5}Zn_{17.5}$ alloy (Fig. 3a). The highest fluctuations of the E_{OCP} during immersion tests in physiological fluid were noticed for $Ca_{60}Mg_{17.5}Zn_{22.5}$ alloy (Fig. 3c).

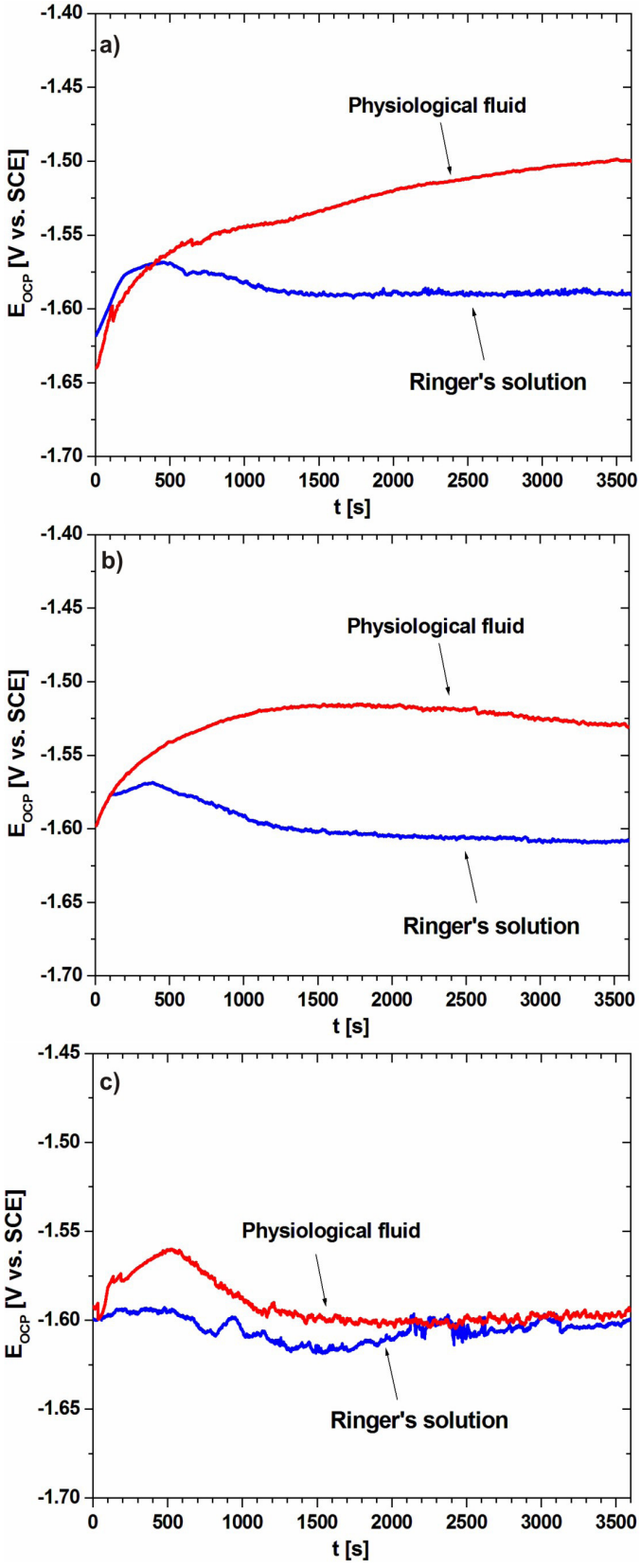

Fig. 3. Variation of the open-circuit potential with time for $Ca_{65}Mg_{17.5}Zn_{17.5}$ (a), $Ca_{62.5}Mg_{17.5}Zn_{20}$ (b), $Ca_{60}Mg_{17.5}Zn_{22.5}$ (c) alloys in Ringer's solution and physiological fluid at 37°C

TABLE 1

The results of corrosion investigations of $Ca_{65-x}Mg_{17.5}Zn_{17.5+x}$ (x = 0, 2.5, 5) metallic glasses in Ringer's solution (E_{OCP} – open-circuit potential, E_{corr} – corrosion potential, R_p – polarization resistance, j_{corr} – corrosion current density)

Sample	E_{OCP} [mV]	E_{corr} [mV]	R_p [Ωcm^2]	j_{corr} [mA/cm^2]
$Ca_{60}Mg_{17.5}Zn_{22.5}$	–1.591±0.03	–1.585±0.03	2.53 ± 0.05	18.82 ± 0.03
$Ca_{62.5}Mg_{17.5}Zn_{20}$	–1.609±0.03	–1.609±0.03	4.82 ± 0.05	11.06 ± 0.03
$Ca_{65}Mg_{17.5}Zn_{17.5}$	–1.598±0.03	–1.602±0.03	3.59 ± 0.05	2.94 ± 0.03

TABLE 2

The results of corrosion investigations of $Ca_{65-x}Mg_{17.5}Zn_{17.5+x}$ (x = 0, 2.5, 5) metallic glasses in physiological fluid (E_{OCP} – open-circuit potential, E_{corr} – corrosion potential, R_p – polarization resistance, j_{corr} – corrosion current density)

Sample	E_{OCP} [mV]	E_{corr} [mV]	R_p [Ωcm^2]	j_{corr} [mA/cm^2]
$Ca_{60}Mg_{17.5}Zn_{22.5}$	–1.499±0.03	–1.477±0.03	20.44±0.05	0.94±0.03
$Ca_{62.5}Mg_{17.5}Zn_{20}$	–1.531±0.03	–1.515±0.03	8.02±0.05	0.72±0.03
$Ca_{65}Mg_{17.5}Zn_{17.5}$	–1.595±0.03	–1.589±0.03	17.17±0.05	0.24±0.03

The electrochemical polarization curves determined in Ringer's solution and physiological fluid recorded for studied alloys are presented in Fig. 4. The corrosion potential (E_{corr}) of $Ca_{65-x}Mg_{17.5}Zn_{17.5+x}$ (x = 0, 2.5, 5) alloys is rather not changed in Ringer's solution. The increase of Zn content in studied alloys caused that values of the E_{corr} are moved to negative potential values in physiological fluid. Based on the Tafel's extrapolation of polarization curves collected in Ringer's solution and physiological fluid corrosion properties were listed in Table 1 and 2, consequently.

The lowest polarization resistance (R_p) with a value of 2.53 Ωcm^2 was determined for alloys tested in Ringer's solution. The highest polarization resistance at a level of 20.44 Ωcm^2 was determined in physiological fluid for $Ca_{60}Mg_{17.5}Zn_{22.5}$ alloy. In addition, the highest polarization resistance (R_p = 4.82 Ωcm^2) in Ringer's solution and the lowest polarization resistance (R_p = 8.02 Ωcm^2) in physiological fluid was noted for $Ca_{62.5}Mg_{17.5}Zn_{20}$ alloy. The corrosion current density (j_{corr}) of samples examined in both corrosive fluids increased with the increase of Zn content. The value of the j_{corr} for all alloys in Ringer's solution is significantly higher than for the same samples tested in physiological fluid.

The XRD patterns of corrosion products formed on surface of $Ca_{65-x}Mg_{17.5}Zn_{17.5+x}$ (x = 0, 2.5, 5 at.%) samples after 1 h of immersion in Ringer's solution at 37°C are presented in Fig. 5. The $Ca(OH)_2$ and $Ca(CO)_3$ phases were mainly detected. Moreover, some peaks come from CaO, $Ca(Zn(OH)_3)_2 \cdot 2H_2O$, $Zn(OH)_2$, CaZn2 and Ca3Zn were also detected after 1 h of immersion in Ringer's solution.

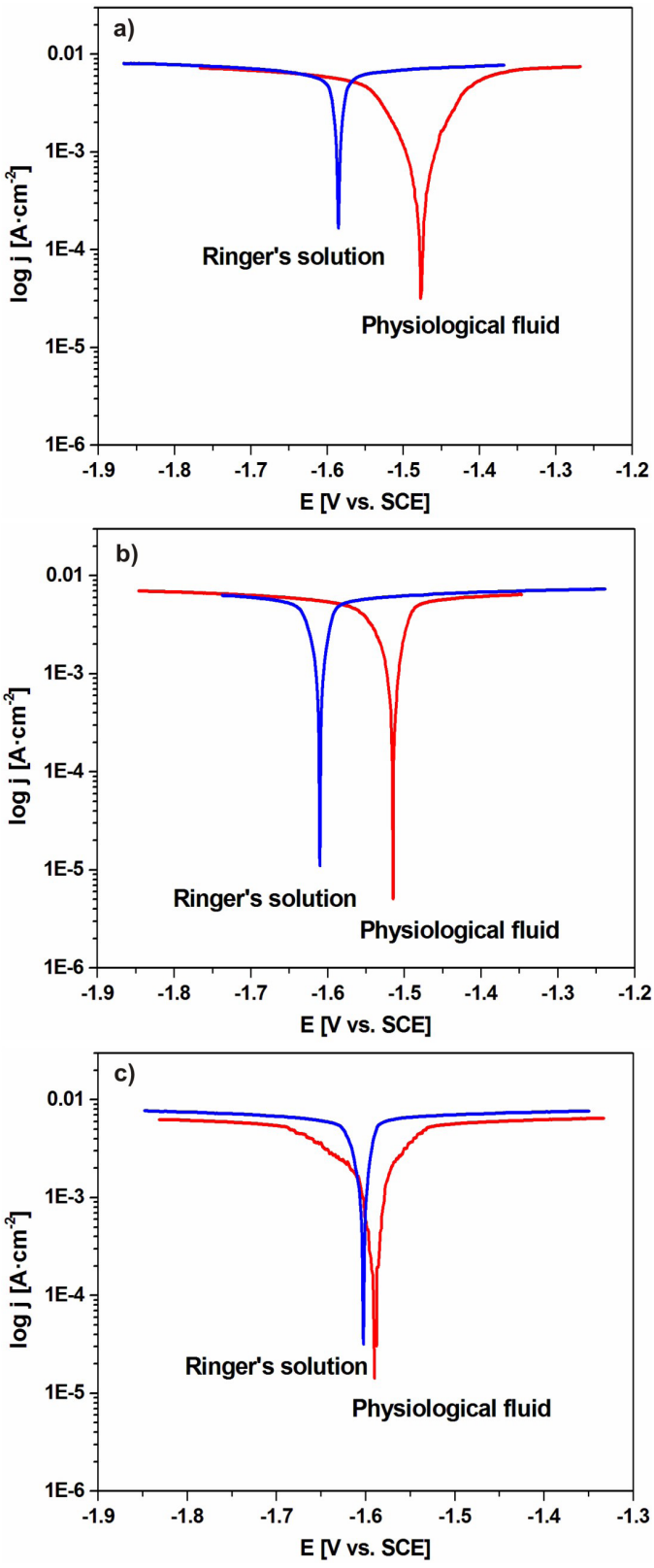

Fig. 4. Polarization curves of $Ca_{65}Mg_{17.5}Zn_{17.5}$ (a), $Ca_{62.5}Mg_{17.5}Zn_{20}$ (b), $Ca_{60}Mg_{17.5}Zn_{22.5}$ (c) alloys in Ringer's solution and physiological fluid at 37°C

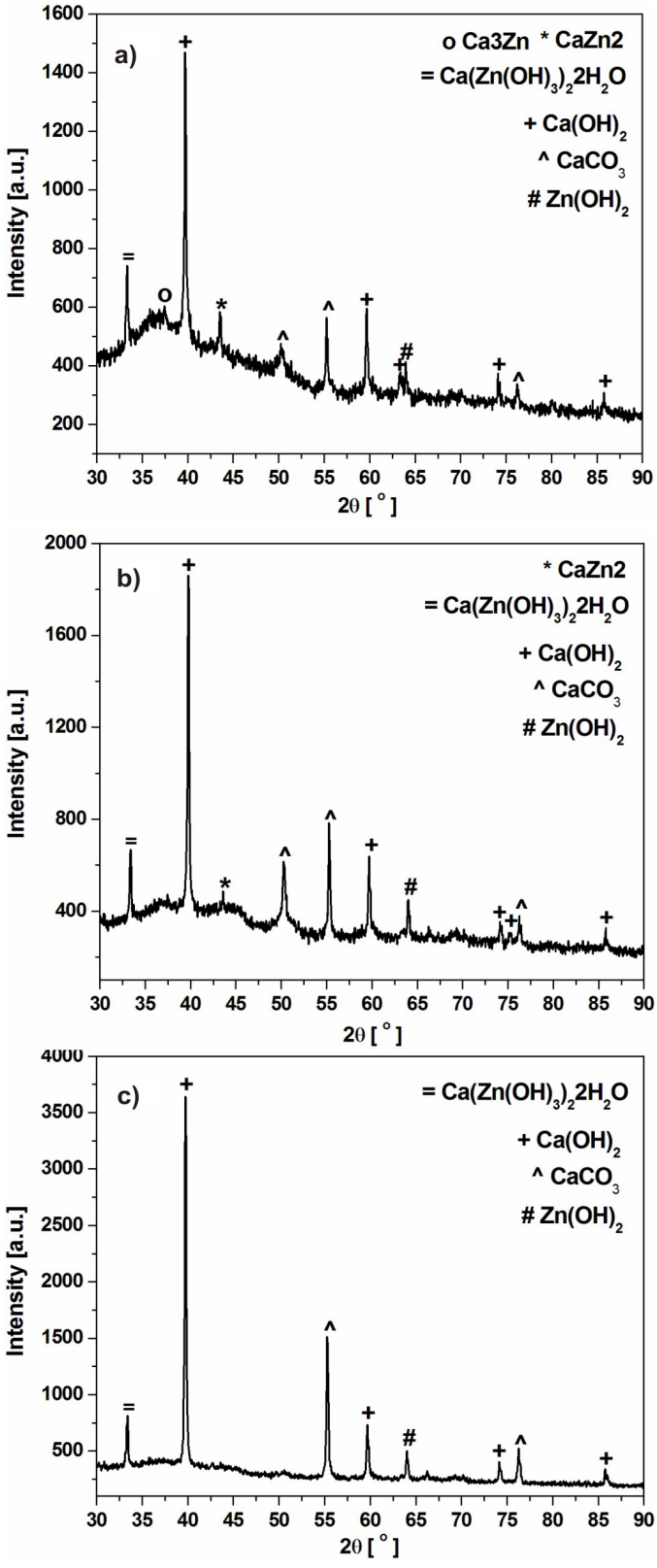

Fig. 5. XRD patterns of $Ca_{65}Mg_{17.5}Zn_{17.5}$ (a), $Ca_{62.5}Mg_{17.5}Zn_{20}$ (b), $Ca_{60}Mg_{17.5}Zn_{22.5}$ (c) samples after 1 h of immersion in Ringer's solution at 37°C

Fig. 6 represents the survey spectra for $Ca_{60}Mg_{17.5}Zn_{22.5}$ alloy after immersion test in Ringer's solution during 1 h. The spectra were determined before and after etching. The characteristic main photoemission lines (e.g.: C1s, O1s, Ca2p, Mg1s, Zn2p) and peaks (O KLL, C KLL, Zn LMM, Mg KLL) corresponding to individual elements are denoted. The dominated contribution is C1s (around 52 at.%) as a surface impurity, which is drastically reduced by Ar^+ beam sputtering to around 10 at.% (Fig. 7).

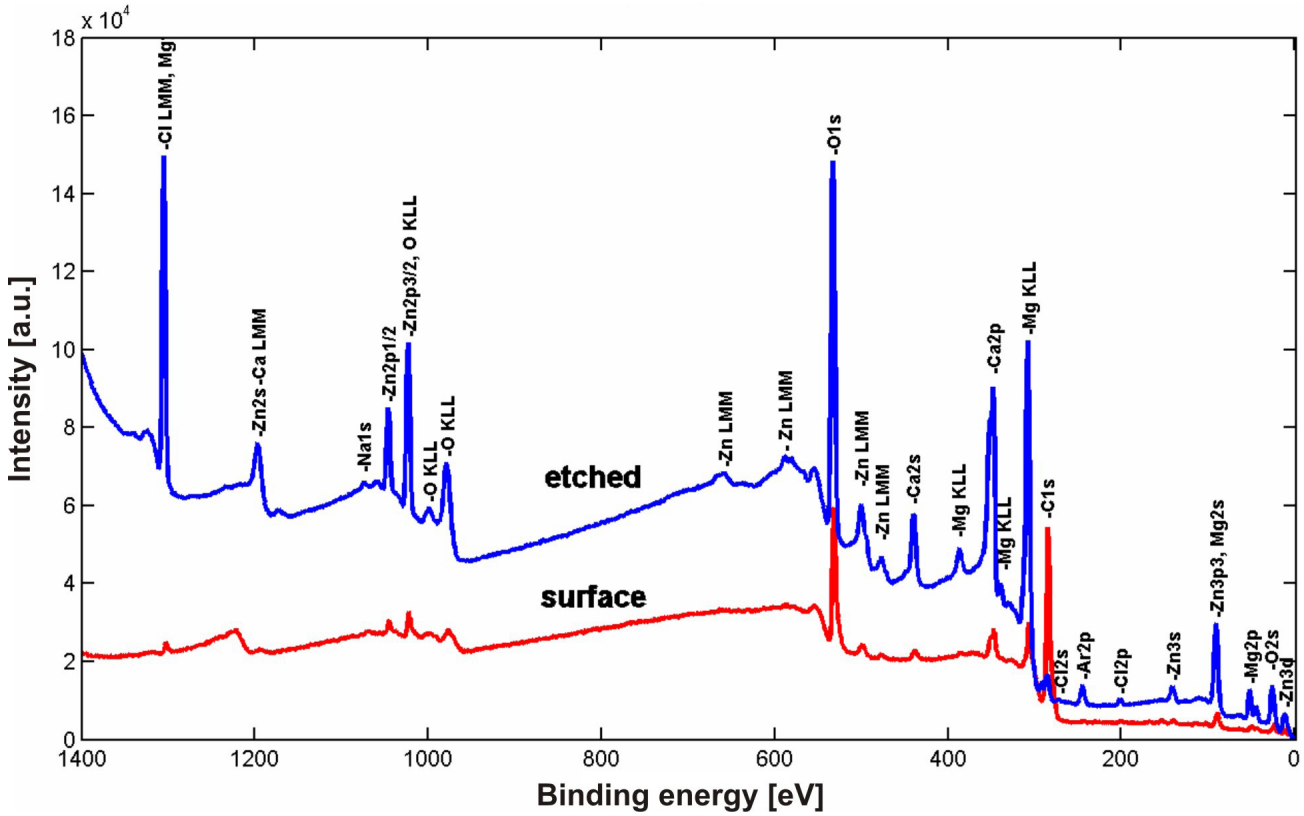

Fig. 6. XPS survey spectra of $Ca_{60}Mg_{17.5}Zn_{22.5}$ alloy after immersion test in Ringer's solution

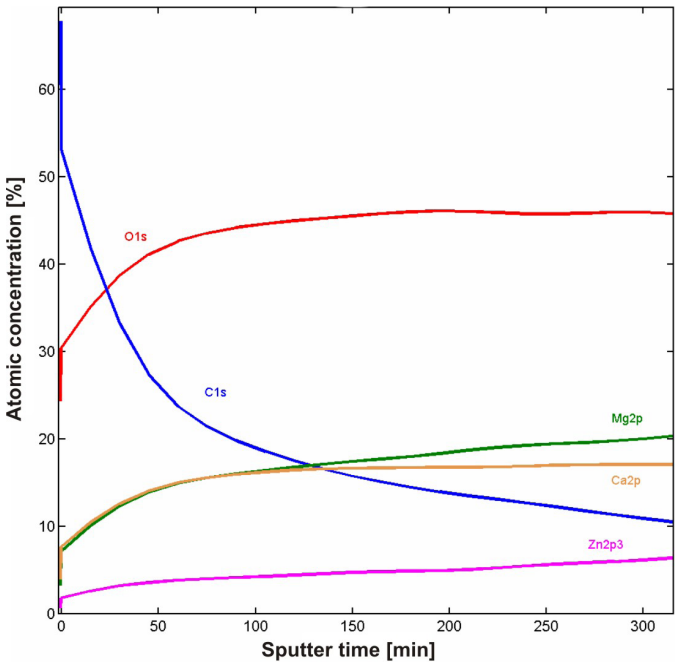

Fig. 7. DP-XPS result of $Ca_{60}Mg_{17.5}Zn_{22.5}$ alloy after immersion test in Ringer's solution

On the other hand the O1s component around 30 at.% the surface is slightly increased to around 45 at.%, which is probably related to various oxides. The atomic concentration of other elements at the surface is relatively low (less than 10 at.%), but they are covered by the surface contaminants like sulfur, silicon, sodium, chloride (Fig. 6). The contribution of two latter ones is even higher for subsurface layers due to the chemical treatment of studied specimen.

The core level lines spectra acquired during DP-XPS procedure for the $Ca_{60}Mg_{17.5}Zn_{22.25}$ alloy after immersion test in Ringer's solution during 1 h are depicted in Fig. 8. First of all on the surface dominates contamination by carbon represents as C1s line (Fig. 8a), which is composed of two peaks. The highest one is associated with carbon – surface component (BE = 284.8 eV), which decreases over ion etching, whereas that with lower intensity (BE ≈ 291.7 eV) may originate from various carbonates, probably mostly $CaCO_3$. The oxygen O1s line (Fig. 8b) on the surface (BE = 531.8 eV) is rather narrow and is subsequently broadened over ion etching. Thus, it may be an effect of overlapping peaks typical for MgO (BE = 531.5 eV, 532.2 eV), CaO (BE = 531.3 eV, 532.2 eV) as well as ZnO (BE = 530.4 eV) states. The calcium Ca2p line is typical for CaO (Fig. 8c) contribution and indicates the spin orbit splitting (L-S) into $Ca2p_{3/2}$ (BE ≈ 347.6 eV) and $Ca2p_{1/2}$ (BE ≈ 351.1 eV) with ΔE ≈ 3.5 eV. During DP-XPS procedure the intensity of Ca2p line is raised, but its binding energy is rather stable pointing to the domination of CaO in the entire sample volume tested. The intensity of Mg2p line is rather low at the surface (Fig. 8d). However, during ion cleaning it becomes much larger. On the surface it can be related to a presence of $Mg(OH)_2$ (BE ≈ 50.1eV) component, whereas after ion cleaning it is rather dominated by MgO (BE ≈ 51.8eV) states. The Mg2p core level line is presented together with Ca3s (BE ≈ 44.1eV) states. The

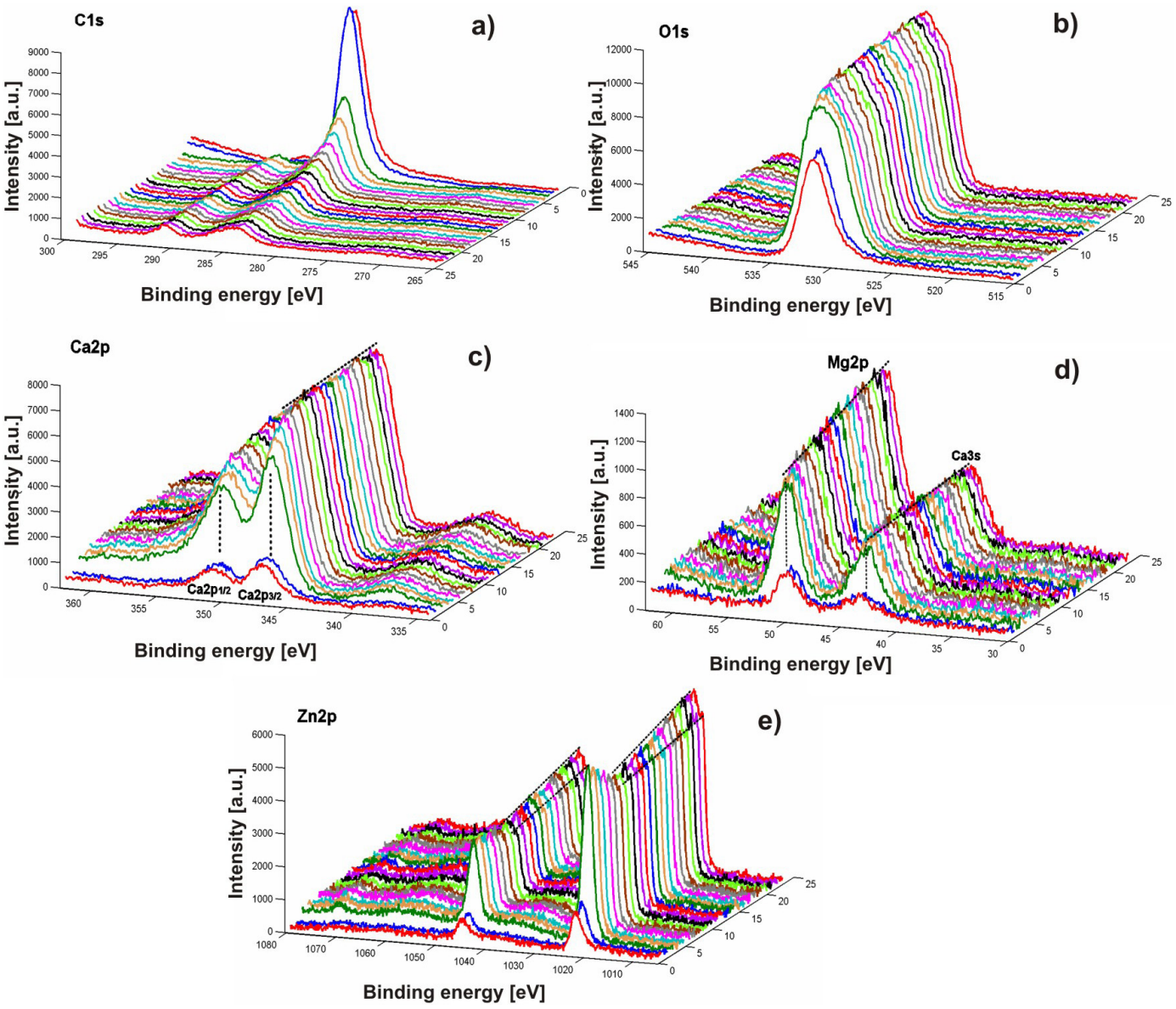

Fig. 8. Core level lines spectra of $Ca_{60}Mg_{17.5}Zn_{22.5}$ alloy after immersion test in Ringer's solution

Zn2p line (Fig. 8e) at the surface is dominated by ZnO. Thus, it is composed of two lines $Zn2p_{3/2}$ (BE ≈ 1022.6eV) and $Zn2p_{1/2}$ (BE ≈ 1045.7eV) with L-S splitting of ΔE ≈ 23.1eV. Over argon beam etching the Zn2p line becomes more complex and one may notice an appearance of additional peaks on the lower binding energy side. It may be related to the presence of pure zinc states ($Zn2p_{3/2}$ – BE ≈ 1021.4eV and $Zn2p_{1/2}$ – BE ≈ 1044.4eV).

The surface morphology of $Ca_{60}Mg_{17.5}Zn_{22.5}$ alloy in as-grinded state is presented in Fig. 9a. For comparison effects of corrosion tests on the surface morphology of studied alloy during 1, 2 and 3 h in Ringer's solution are presented in Fig. 9b,c,d. Microscopic observations allowed to state that the corrosion of samples increases with immersion time. After 1 h of immersion single pits and corrosion products can be observed on the sample surface (Fig. 9b). After 2 h of immersion the alloy surface was covered by thick corrosion products layer (Fig. 9b). The corrosion layer mainly contained calcium oxides and hydroxides as it was verified by results of XRD and XPS measurements. The corrosion layer exhibited a very weak stability in Ringer's solution, therefore the corrosion resistance was also very low. What is more, the characteristic corroded areas after 3 h of immersion as a result of hydrogen evolution on the specimen surface can be observed (Fig. 9d).

4. Discussion

It is important to note that corrosion behavior of Ca-based alloys depends on structure, chemical composition of material as well as properties of corrosion products layer formed during immersion in different corrosive solutions. In this work, the hydrogen evolution volume decreases with the increase of Zn content for alloys tested in Ringer's solution. However, volume of the H_2 and corrosion current increased with the decrease of Zn content of Ca-based alloys tested in the minimum essential medium (MEM) [2].

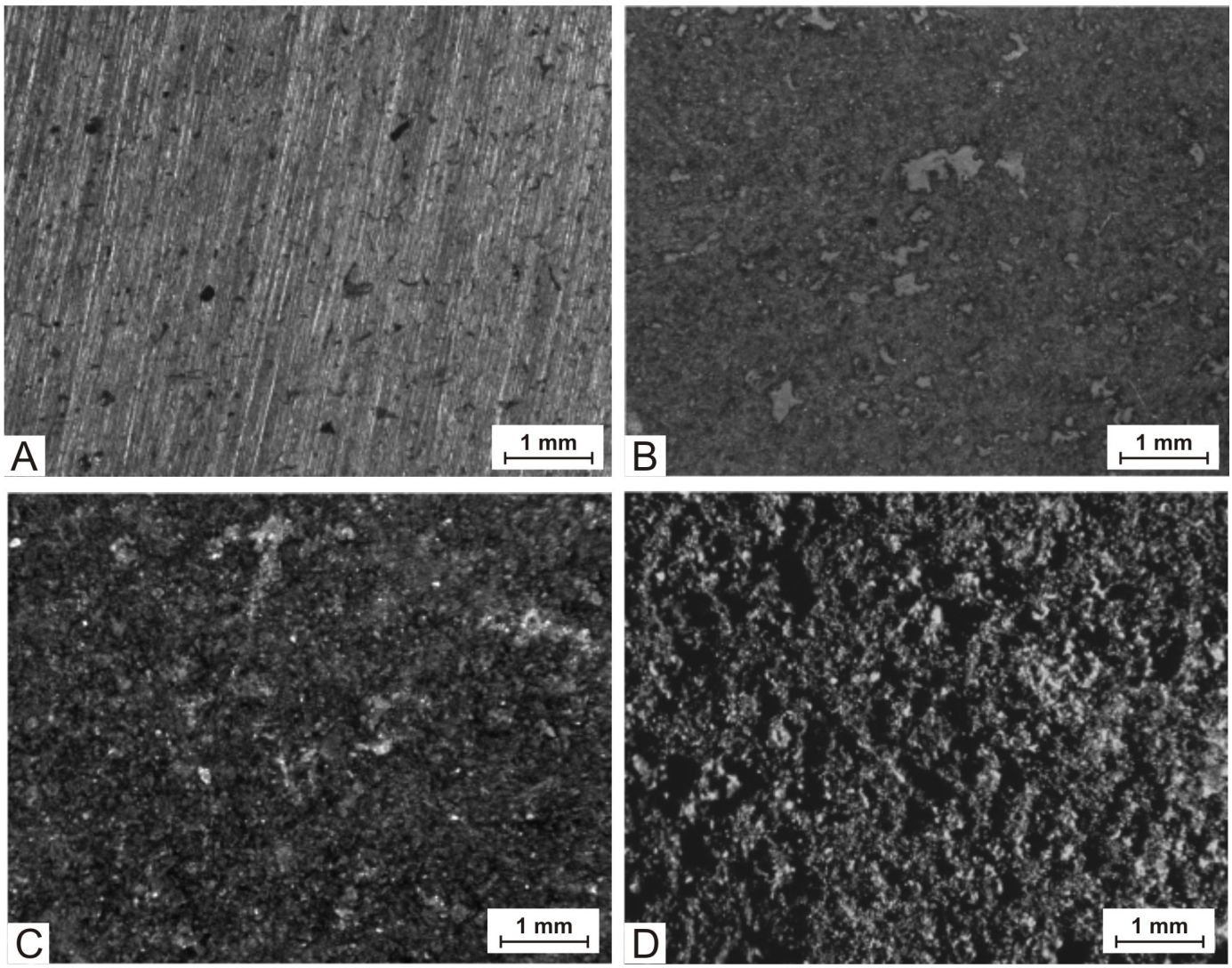

Fig. 9. Micrographs of the surface morphology of $Ca_{60}Mg_{17.5}Zn_{22.5}$ in as-cast state (a) and after immersion tests in Ringer's solution during 1 h (b), 2 h (c) and 3 h (d) at 37°C

For comparison, in work [27] hydrogen evolution volume determined after 10 h of immersion in distilled water for $Ca_{60}Mg_{15}Zn_{25}$ alloy exhibited a value of 100 ml/cm^2. After immersion in Hank's solution during 200 min a volume of the H_2 for $Ca_{65}Mg_{15}Zn_{20}$ metallic glass exhibited a value of about 35 ml/cm^2 [3]. In present paper hydrogen volume determined in Ringer's solution for $Ca_{62.5}Mg_{17.5}Zn_{20}$ alloy with similar chemical composition showed a value of 15 ml/cm^2.

The slightly changes of the E_{OCP} during immersion tests in physiological fluid were noticed for $Ca_{65}Mg_{17.5}Zn_{17.5}$ alloy (Fig. 3a). For the $Ca_{60}Mg_{17.5}Zn_{22.5}$ alloy the highest fluctuations of the E_{OCP} during immersion tests in physiological fluid were observed (Fig. 3c). The $Ca_{60}Mg_{17.5}Zn_{22.5}$ alloy manifested an amorphous structure with some crystalline phases (probably CaZn2 and Ca3Zn). We can assume that the small amount of crystalline phases and difference chemical composition of studied alloys caused a change of their electrochemical activity. It should be noticed, that any amount of the crystallinity decreases resistance of the oxidation supplying both boundaries and composition inhomogeneity.

Results of potentiodynamic studies (Fig. 3,4) indicated, that changes of Zn content in studied Ca-based alloys caused differences in kinetics of the open-circuit potential and polarization curves. The largest variations of the E_{OCP} in a function of time were recorded for $Ca_{60}Mg_{17.5}Zn_{22.5}$ alloy. In addition, the difference of structure in as-cast state among studied alloys had an impact on chemical composition and structure of oxidation layers. Consequently, the chemical composition and structure oxidation surface layers affects on kinetics of potentiodynamic tests.

The XRD patterns of $Ca_{65-x}Mg_{17.5}Zn_{17.5+x}$ (x = 0, 2.5, 5 at.%) samples after immersion tests indicated, that $Ca(OH)_2$ and $Ca(CO)_3$ phases were mainly present on surface of alloys (Fig. 5). In addition, the XRD patterns of $Ca_{60}Mg_{17.5}Zn_{22.5}$ alloy indicated more crystalline character than for $Ca_{65}Mg_{17.5}Zn_{17.5}$ and $Ca_{62.5}Mg_{17.5}Zn_{20}$ alloys, consequently. The corrosion products formed on surface of $Ca_{65-x}Mg_{17.5}Zn_{17.5+x}$ (x = 0, 2.5, 5 at.%) samples after 1 h of immersion in Ringer's solution were identified as MgO, CaO, $Ca(OH)_2$, $Zn(OH)_2$, $CaCO_3$. During immersion in aqueous Ringer's solution Ca dissoluted to Ca^{2+}. The atoms diffused and reacted with hydroxyl ions OH^- form

a layer of $Ca(OH)_2$. The calcium carbonate was detected as corrosion products, probably due to reaction of Ca atoms from the dissolute alloy with carbon dioxide coming from the air. The particles of calcium carbonate in corrosive solution dropped out on the sample surface. The $CaCO_3$ layer is stable at alkaline pH of corrosive solution [28]. The solution with alkaline pH is mainly produced by the evolved hydrogen and a formation of hydroxyl groups (OH) [29].

5. Conclusions

The changes of open-circuit potential and hydrogen evolution volume indicated that studied Ca-based alloys are active materials. The hydrogen volume decreased with the increase of Zn content of Ca-based alloys in Ringer's solution. These results can give an opportunity to used them as biomaterials. However, the increasing tendency of corrosion current density was noted for samples with the highest Zn content (22.5 at.%). The corrosion products after immersion tests in Ringer's solution were identified by X-ray diffraction and X-ray photoelectron spectroscopy as calcium/magnesium oxides, carbonates, hydroxides and calcium hydrate. Therefore, the further experiments should be conducted in case of decrease the corrosion activity by applying protective layers.

Acknowledgements

The work was supported by the Faculty of Mechanical Engineering, Silesian University of Technology statutory grants in 2018 and partially supported by National Science Centre under research project no.: 2013/09/B/ST8/02129.

REFERENCES

[1] A. Takeuchi, A. Inoue, Mater. Trans. **46**, 2817-2829 (2005), DOI: 10.2320/matertrans.46.2817.

[2] S. Cai, T. Lei, N. Li, F. Feng, Mater. Sci. Eng. C **32**, 2570-2577 (2012), DOI: 10.1016/j.msec.2012.07.042.

[3] H.R.B. Rad, M.H. Idris, M.R.A. Kadir, S. Farahany, Mater. Des. **33**, 88-97 (2012), DOI: 10.1016/j.matdes.2011.06.057.

[4] J.D. Cao, N.T. Kirkland, K.J. Laws, N. Birbilis, M. Ferry, Acta Biomater. **8**, 2375-2383 (2012) , DOI: 10.1016/j.actbio.2012.03.009.

[5] Y.B. Wang, X.H. Xie, H.F. Li, X.L. Wang, M.Z. Zhao, E.W. Zhang, Y.J. Bai, Y.F. Zheng, L. Qin, Acta Biomater. **7**, 3196-3208 (2011), DOI: 10.1016/j.actbio.2011.04.027.

[6] A. Monfared, A. Ghaee, S. Ebrahimi-Barough, J. Non-Cryst. Solids **489**, 71-76 (2018), DOI: 10.1016/j.jnoncrysol.2018.03.031.

[7] O. Baulin, D. Fabrègue, H. Kato, A. Liens, T. Wada, J, M. Pelletier, J. Non-Cryst. Solids **481**, 397-402 (2018), DOI: 10.1016/j.jnoncrysol.2017.11.024.

[8] M.K. Datta, D. Chou, D. Hong, P. Saha, S.J. Chung, B. Lee, A. Sirinterlikci, M. Ramanatha, A. Roy, P. Kumta, Mater. Sci. Eng. B **176**, 1637-1643 (2011), DOI: 10.1016/j.mseb.2011.08.008.

[9] N. Hua, W. Chen, Q. Wang, Q. Guo, Y. Huang, T. Zhang, J. All. Compd. **745**, 111-120 (2018), DOI: 10.1016/j.jallcom.2018.02.138.

[10] W. Jiao, K. Zhao, X.K. Xi, D.Q. Zhao, M.X. Pan, W.H. Wang, J. Non-Cryst. Solids **356**, 1867-1870 (2010), DOI: 10.1016/j.jnoncrysol.2010.07.017.

[11] W. Jiao, H.F. Li, K. Zhao, H.Y. Bai, Y.B. Wang, Y.F. Zheng, J. Non-Cryst. Solids **357**, 3830-3840 (2011), DOI: 10.1016/j.jnoncrysol.2011.08.003.

[12] K. Zhao, J. F. Li, D. Q. Zhao, M. X. Pan, W. H. Wang, Scripta Mater. **61**, 1091-1094 (2009), DOI: 10.1016/j.scriptamat.2009.08.042.

[13] Y.B. Wang, H.F. Li, Y.F. Zheng, M. Li, Mater. Sci. Eng. C **32**, 599-606 (2012), DOI: 10.1016/j.msec.2011.12.018.

[14] C.L. Qin, Q.F. Hu, Y.Y. Li, Z.F. Wang, W.M. Zhao, D.V. Louzguine-Luzgin, A. Inoue, Mater. Sci. Eng. C **69**, 513-521 (2016), DOI: 10.1016/j.msec.2016.07.022.

[15] O. Baulin, D. Fabrègue, H. Kato, T. Wada, S. Balvay, D.J. Hartmann, J. Pelletier, J. Non-Cryst. Solids **500**, 78-83 (2018), DOI: 10.1016/j.jnoncrysol.2018.06.026.

[16] K. Han, J. Qiang, Y. Wang, P. Häussler, J. All. Compd. **729**, 144-149 (2017), DOI: 10.1016/j.jallcom.2017.09.144.

[17] H.F. Li, X.H. Xie, K. Zhao, Y.B. Wang, Y.F. Zheng, W.H. Wang, L. Qin, Acta Biomater. **9**, 8561-8573 (2013), DOI: 10.1016/j.actbio.2013.01.029.

[18] H.F. Li, K. Zhao, Y.B. Wang, Y.F. Zheng, W.H. Wang, J. Biomed Mater. Res. B Appl. Biomater. **100**, 368-377 (2012), DOI: 10.1002/jbm.b.31958.

[19] R. Nowosielski, A. Bajorek, R. Babilas, J. Non-Cryst. Solids **447**, 126-133 (2016), DOI: 10.1016/j.jnoncrysol.2016.05.037.

[20] L. Hu, B.Y. Liu, F. Ye, B.C. Wei, G.L. Chen, Intermetallics **19**, 662-665 (2011), DOI: 10.1016/j.intermet.2011.01.003.

[21] B. Zberg, P.J. Uggowitzer, J.F. Löffler, Nature Mater. **8**, 887 (2009), DOI: 10.1038/nmat2542.

[22] J. Schroers, G. Kumar, T. M. Hodges, S. Chan, T.R. Kyriakides, JOM **61**, 21-29 (2009), DOI: 10.1007/s11837-009-0128-1.

[23] H.F. Li, Y.F. Zheng, Acta Biomater. **36**, 1-20 (2016), DOI: 10.1016/j.actbio.2016.03.047.

[24] E.S. Park, D.H. Kim, Met. Mater. Int. **11**, 19 (2005), DOI: 10.1007/BF03027480.

[25] O.N. Senkov, J.M. Scott, J. Non-Cryst. Solids **351**, 3087-3094 (2005), DOI: 10.1016/j.jnoncrysol.2005.07.022.

[26] S. Gorsse, G. Orveillon, O. N. Senkov, and D. B. Miracle, Phys. Rev. B **73**, 1-33 (2006), DOI: 10.1103/PhysRevB.73.224202.

[27] H.F. Li, Y.B. Wang, Y. Cheng, Y.F. Zheng, Mater. Let. **64**, 1462-1464 (2010), DOI: 10.1016/j.matlet.2010.03.060.

[28] S. Feliu (Jr), I. Lorente, Appl. Surf. Sci. **347**, 736-746 (2015), DOI: 10.1016/j.apsusc.2015.04.189.

[29] G. Song, Corrosion Prevention of Magnesium Alloys, 1-st ed., Woodhead Publishing limited, Philadelphia, 2013.